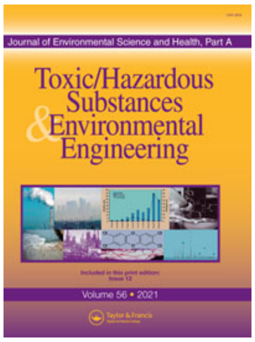

Taylor & Francis
Taylor & Francis Group

Journal of Environmental Science and Health, Part A
Toxic/Hazardous Substances and Environmental Engineering

ISSN: (Print) (Online) Journal homepage: https://www.tandfonline.com/loi/lesa20

A milliseconds flash joule heating method for the regeneration of spent cathode carbon

Pengfei Huang, Rongtao Zhu, Xinxi Zhang & Wenjun Zhang

To cite this article: Pengfei Huang, Rongtao Zhu, Xinxi Zhang & Wenjun Zhang (2022): A milliseconds flash joule heating method for the regeneration of spent cathode carbon, Journal of Environmental Science and Health, Part A, DOI: 10.1080/10934529.2021.2022422

To link to this article: https://doi.org/10.1080/10934529.2021.2022422

JOURNAL OF ENVIRONMENTAL SCIENCE AND HEALTH, PART A
https://doi.org/10.1080/10934529.2021.2022422

A milliseconds flash joule heating method for the regeneration of spent cathode carbon

Pengfei Huang[a], Rongtao Zhu[a,b], Xinxi Zhang[a,b], and Wenjun Zhang[b]

[a]Key Laboratory of Coal Processing and Efficient Utilization of Ministry of Education, China University of Mining and Technology, Xuzhou, Jiangsu, China; [b]School of Chemical Engineering and Technology, China University of Mining and Technology, Xuzhou, Jiangsu, China

ABSTRACT
Spent cathode carbon (SCC) blocks of aluminum electrolytic cell were hazardous waste produced in the production of electrolytic aluminum. In this present work, a facile, rapid, and economical strategy was proposed to remove fluoride and other toxic substances in the SCC block by the flash joule heating method. SCC after flash joule heating (F-SCC) were prepared in different flash voltages and number of passes; the chemical composition, microscopic morphology and carbon configuration of the SCC and F-SCC were described in detail. The results show that the purification efficiency depends upon the flash voltages and pass number. In terms of flash voltage, 150 V (5.62 kJ/g) is the optimal voltage to maintain the micro-expansion characteristics of the cathode carbon. Multiple flash joule heating can not only maintain its high-graphitization carbon, but also improve its micro-expansion characteristics. In addition, the electrochemical performance of F-SCC was characterized, and F-SCC displayed excellence capacitance performance. The low-cost, rapid -regeneration method based on the flash joule heating provides an effective method for the clean recycling and high-value utilization of carbonized solid waste.

ARTICLE HISTORY
Received 14 September 2021
Accepted 12 December 2021

KEYWORDS
Spent cathode carbon; flash joule heating; purification; capacitance performance

Introduction

Spent cathode carbon (SCC), as a solid waste produced in the aluminum electrolysis industry, is fast growing due to the increasing demand for aluminum in the world.[1] Cathode carbon is inevitably corroded by high-temperature electrolytes, molten aluminum, metallic sodium, and other substances during the working process.[2–4] Therefore, SCC is composed of fluorinated carbon, alumina, cryolite, aluminosilicate, trace cyanide (0.2–1 wt%), and other substances in the waste pot lining (SPL).[5–7] The carbon of high-graphitization and micro-expansion endows SCC with a high-quality recycling value. Meanwhile, the cyanide and fluoride, if left untreated, would seriously damage the environment and ecology.[8,9]

Over the last few years, much has been done in the field of SCC recovery for its toxicity and recyclability in the world.[10–13] And generally, there are three conventional methods of SCC recovery: leaching process,[11,14–16] roasting method[10,12,13] and vacuum distillation process.[17,18] First, the leaching process is mainly to extract soluble fluoride from SCC in a solution environment of water, caustic, and acid. However, this method may easily cause severe corrosion of SCC processing equipment because corrosive solutions (such as NaOH and HCl) or the generated harmful gases (such as HF) are used in the process. Besides, the process may last several hours and requires complicated post-processing procedures (such as drying and waste liquid treatment).[19,20] Secondly, the traditional roasting method[12] is to burn carbide at high temperatures. In this process, high-graphitization carbon is used as fuel, which not only wastes carbon resources but also produces useless spent residue. And thirdly, the vacuum distillation method can separate the carbon in SCC while removing its impurities, but it is featured by high energy consumption and a long process cycle.[21] In short, all the above-mentioned separation and utilization methods are not satisfactory due to the existing shortcomings, such as high energy consumption, long process time, low added value, and environmental pollution.

At present, the potential application of high-graphitization and micro-expansion carbon materials in the purification SCC in the electrode material of supercapacitors has not attracted widespread attention. The high-graphitization of SCC leads to its high conductivity as an electrode of supercapacitor, and the micro-expansion graphite layered crystal domains in the iso-oriented allow reversible intercalation of both cations and anions.[22] Meanwhile, metals such as Al and Fe in SCC show that the energy storage level of redox pseudocapacitors can be increased.[23]

To overcome the shortcomings of the existing SCC purification process, this study proposed a method based on flash joule heating to quickly remove the impurities in SCC and retain the high-graphitization and micro-expansion characteristics of the original SCC. The removal efficiency of

CONTACT Rongtao Zhu rtzhu2010@cumt.edu.cn; Xinxi Zhang zhangxinxi@126.com Key Laboratory of Coal Processing and Efficient Utilization of Ministry of Education, China University of Mining and Technology, Xuzhou 221116, Jiangsu, China.

impurities in SCC was explored under different flash joule heating voltages and processing passes. At the same time, the electrochemical characteristics of purified SCC were evaluated as a supercapacitor electrode material. This method could provide an effective way for the clean recycling and high-value utilization of carbonized solid waste. More importantly, SCC recycling and processing technology support the resource recycling and sustainable development of the aluminum reduction industry.

The innovative high-temperature thermal shock (HTS) technology was based on electric Joule heating, and the entire HTS process lasts only a few milliseconds.[24,25] Compared with traditional thermal radiation heating, it is more environmentally friendly and energy-saving. More importantly, it can fully retain and improve the structural advantages of SCC carbon materials (such as high-graphitization and micro-expansion), thus maximizing the value of SCC.

Experimental approaches

Materials and methods

The circuit diagram of the flash joule heating system is shown in Figure A1 in the supporting information. The system is composed of a control module, a charging module, a discharging module, a workpiece module, an energy storage module, a measurement module, and a sample stage. The raw materials were processed in the following procedures. Before the treatment of flash joule heating, SCC (Henan Province, China) was ground into powder by a crusher. The powder smaller than 200-mesh (0.074 mm) was screened out for the next flash joule heating, as shown in Figure 2b. Then 120 mg of crushed SCC (200 mesh) was accurately weighed with an analytical balance and placed into a glass tube (length 50 mm, inner diameter 6 mm, wall thickness 2 mm), and the two end surfaces were sealed with graphite blocks. Since the gap between the graphite block and the glass tube renders a poor sealing performance, a layer of conductive copper tape was attached to the graphite block to prevent the broken SCC powder from escaping, as shown in Figure 1c. Finally, SCC was regenerated with a flash joule heating system under different voltages (100 V, 150 V, 200 V) and number of processing passes (1,3,5), and named SCC, SCC-100, SCC-150, SCC-200, SCC-150-3 and SCC-150-5, respectively. The SCC after flash joule heating was denoted as F-SCC. The flash joule heating device used in this experiment has a capacitor bank with a capacitance of 60 mF and a voltage of 0–450 V, and the discharge time is set to 500 ms so that the electricity in the capacitor can be completely discharged. In such a short time, the reaction temperature can reach an ultra-high level (>3000 K) immediately, and the heating/cooling rate is 10^5 K s^{-1}.[26]

Material characterization

The morphology and microstructure of SCC and F-SCC were studied by SEM (MAIA3 LMH, USA) and the energy dispersive X-ray analysis (EDX, MAIA3 LMH, USA) was applied for the detection of elemental dispersion on the SCC surface. X-ray powder diffraction (XRD) was conducted at room temperature by using a Bruker D-8 Advance diffractometer (USA) with nickel-filtered Cu Kα ($\lambda = 1.54178$ Å) radiation and the data were collected from 5° to 80° with a scan rate of 2° min^{-1} to obtain the phase structure of SCC and Flash-SCC. Raman measurements were done for the composite by a Raman spectrometer (Senterra, Bruker, Germany) equipped with a 532 nm laser line to determine the chemical composition and structure of SCC. XRF (X-Ray Fluorite Spectroscopy S8 Tiger, Bruker, Germany) was used for the analysis and detection of its detailed chemical elements.

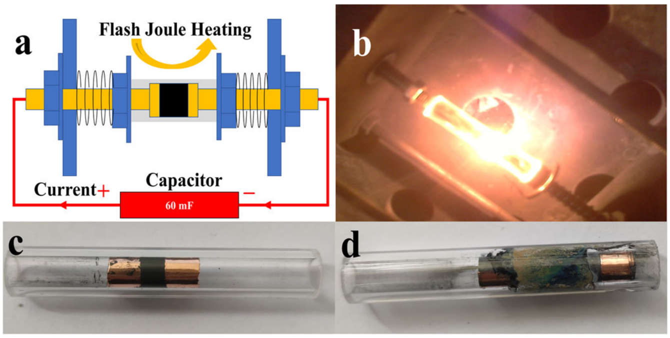

Figure 1. (a) Schematic diagram of flashing Joule heating device (b) Flash process (c) sample of SCC before and (d) after flash joule heating.

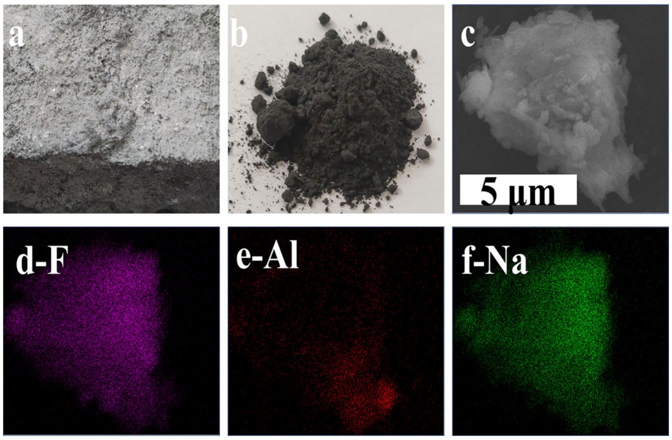

Figure 2. (a) Topography of SCC in aluminum reduction cell, (b) Topography of SCC after crushing, SEM micrograph of initial SCC (a) element distribution map of F(b), Na(c), Al(d).

Molecular dynamics simulation

All molecular dynamics simulations used in this study were performed by the Materials Studio simulation package (accelrys software). From Table 1, it can be known that more than 90% of the elements in the waste cathode carbon are composed of C, F, and Na. Among them, the C element is mainly composed of aromatic compounds in the graphite phase; F and Na are mainly composed of NaF. The system was set to graphite layer and NaF layer to simulate the diffusion of NaF in the graphite layer. The initial configuration was $C_{588}F_{128}Na_{128}$, consisting of six layers of graphite flakes

Table 1. Analysis of the content of chemical elements in SCC.

Elements	C	F	Na	Ca	Al	others
Contents/wt %	65.19	13.97	11.99	2.68	3.96	2.21

and four layers of NaF ($a = 18.00$ Å, $b = 18.00$ Å, $c = 29.00$ Å), and periodic boundary conditions were applied in all directions. Based on the constructed system, the compass potential field and the atomic group-based "Group-based" system were selected to calculate the interaction force. "Atom-Based" module and "Ewald" module were chosen to calculate van der Waals force and electrostatic force between particles.

After constructing the lattice structure, the established lattice structure was optimized by these two functions: "Geometry Optimization" and "Anneal". On this basis, a stable lattice was obtained to solve the trajectory of molecular motion. According to the "Dynamic" function of the software, a 20 ps NVT (number of atoms, volume, and temperature) dynamic simulation was performed on the constructed lattice system, and the result of the balanced lattice model structure system and the movement trajectory of various particles could be obtained.

The calculation Equation of the diffusion coefficient is as follows:

$$D = \frac{1}{6N} \lim_{t\to\infty} \frac{d}{dt} \sum_{i=1}^{N} \left\{ [r_i(t) - r_0(t)]^2 \right\} \tag{1}$$

where N represents the number of diffused atoms in the system, and t denotes the movement time of the particles. For a particle that walks randomly in Brownian motion, the average of the square of its moving distance is proportional to the moving time. Since the mean square displacement (MSD) value in Materials studio is defined, and the diffuse atom N has been averaged, it can be obtained: $D = a/6$, where a denotes the slope of the MSD curve.

Electrochemical measurement

The electrochemical performance was evaluated by using electrochemical workstation (Wuhan Corrtest Instruments Corp., Ltd, China, CS660). To prepare the working electrode, the weight ratio of SCC and Polyvinylidene Fluoride (PVDF, 98%, Sigma-Aldrich) was set to be 90:10, and they were mixed with a mortar and pestle in N-Methyl-2-Pyrrolidone (NMP, $\geq$99%, Sinopharm Chemical Reagent Co., Ltd., China). Then, the resulting uniform slurry was coated on pure copper foil (99.9%) and dried in a vacuum oven at 80 °C for 10 hours. The typical mass load of the electrode obtained was 1.0–1.5 mg cm^{-2}. The electrolyte was a 2 M KOH solution; Ag/AgCl and a platinum sheet were used as the reference electrode and the counter electrode, respectively. Subsequently, the charge and discharge measurement of the electrode was a constant current test in the range of 0.001–1 V vs. Ag/AgCl at room temperature, and the cyclic voltammetry (CV) and electrochemical impedance spectroscopy (EIS) measurements were performed on an electrochemical workstation. CV was performed at a scan rate of 0.01–0.1 mV s^{-1} and EIS was collected by applying a sine wave with an amplitude of 10.0 mV in the frequency range of 100 kHz to 10^{-2} Hz.

Results and discussion

Structure and morphology of SCC

The SCC sample was obtained from an abandoned aluminum electrolytic cell that was removed from an aluminum smelter. The electrolytic cell has been running for 5 years and then damaged, and its morphological characteristics were shown in Figure 2a. Its chemical elements were analyzed and detected by XRF, whose results were listed in Table 1 below. As can be seen from the table, the chemical elements such as C, F, Na, Ca, and Al were the main constituent elements of SCC; and the content of F reached up to about 13.97 wt%. In addition, the C content was 65.19 wt% in SCC, which was consistent with the C content measured in EDX (in Figure A2) and thermal analysis (see Figure A3 in Appendix A).[12,15,17]

The microscopic morphology and chemical composition were analyzed by scanning electron microscope (SEM) and energy dispersive spectrometer (EDS). First, the result of Figure 2c shows that the surface of SCC is covered by many dispersed white substances. Combined with the XRD data in Figure 3, it can be proved that these scattered white substances are different from carbon, and their main ingredients are sodium fluoride (NaF) and calcium fluoride (CaF_2),[27] aluminum oxide (Al_2O_3)[28] and fluorinated aluminum silicate. Besides, although these impurities are subject to physical adhesion (Van der Waals force), due to their combination on a micro-scale, they firmly adhere to the carbon particles. In this case, these impurities cannot be removed from carbon materials effectively by simple physical processes. Furthermore, the EDS analysis in Figures 2d–f shows that the distribution of impurities measured at different positions is not uniform. To be specific, fluoride mainly exists in the crystalline phases of NaF (boiling point 1966 K), CaF_2 (boiling point 2806 K), and Na_3AlF_6 (melting point 1282 K, boiling point: decomposes).[29] When heated to above 1273 K, Na_3AlF_6 decomposes into NaF and AlF_3, and AlF_3 sublimates and escapes at 1273 K.

$$Na_3AlF_6 \overset{1273K}{\rightarrow} 3NaF + AlF_3(\uparrow) \tag{2}$$

Therefore, SCC sublimates impurities through the high temperature (3000 K) generated by the flash Joule heating device and further strengthens its highly graphitized structure. At the same time, the rapid heating and annealing ratio can retain its high-graphitization and micro-expansion structure.[30]

Electrical signal analysis

The instantaneous power P(t) during the Joule thermal shock and the Joule heat Q(t) during the discharge process are of great significance for understanding the cathode carbon purification process. The calculation equation is as follows:

$$P(t) = U(t)I(t) \tag{3}$$

$$Q(t) = \int_0^t U(t)I(t)\mathrm{d}t \tag{4}$$

where: *P(t)* denotes the instantaneous power, W; *U(t)* refers to the instantaneous voltage, V; *I(t)* represents the instantaneous current, A; *Q(t)* is the deposited energy, J; t denotes the time, s.

The energy conversion efficiency refers to the percentage of the maximum energy deposited by the cathode carbon in the energy storage capacitor during the Joule thermal shock. The maximum energy deposited in the cathode carbon can be calculated by Eq. (5), and the energy in the energy storage capacitor can be calculated according to Eq. (6). Accordingly, the energy conversion rate can be obtained by Eq. (7).

$$Q_{\max} = \int_0^{t_{\max}} U(t)I(t)\mathrm{d}t \tag{5}$$

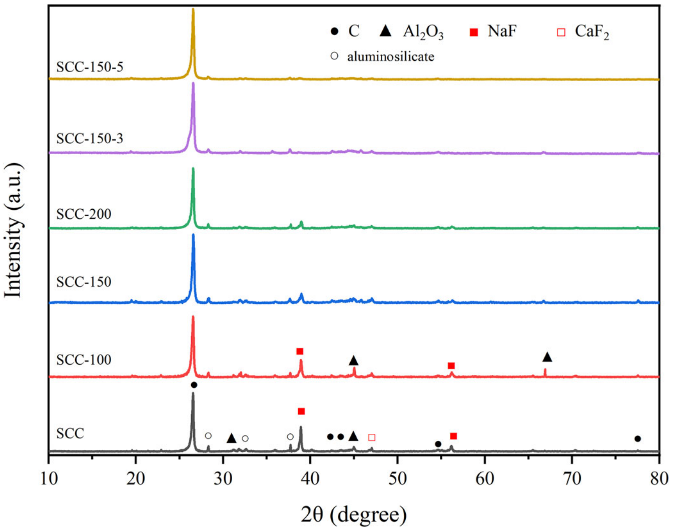

Figure 3. X-ray diffraction patterns of SCC with different flashing voltages and flashing times.

$$W = \frac{1}{2}CU^2 \tag{6}$$

$$\varphi_{\max} = \frac{Q_{\max}}{W} \times 100\% \qquad (7$$

where $Q_{\max}$ is the maximum deposited energy in the SCC, J; *W* denotes the energy stored in the energy storage capacitor, J; *C* refers to the capacitance, 60mF; *U* is the voltage, 100–200 V; $\varphi_{\max}$ stands for the maximum energy conversion rate, %.

The voltage, current, and temperature waveforms were tested during the Joule thermal shock to study their change laws in this process, and the results are shown in Figure 4. Before the discharge switch is turned on, the voltage and current waveforms are both at 0; the instantaneous voltage rises rapidly from 0 V to the peak value as the discharge switch is turned on. Ringback stage: The overshoot voltage decays rapidly in an oscillating wave close to the preset capacitor voltage (here 150 V) and remains stable for a period of time. In this stage, the current waveform fluctuates around 0 A. Thermal shock stage: When a discharge channel is formed inside the sample, electrical energy is injected into the sample instantaneously. Consequently, the voltage across the sample starts to drop from the preset value, and the current waveform also starts to rise at the same time, indicating that a discharge channel has been formed inside the sample. When the current waveform rises to the peak value, it starts to drop until reaching zero, which is caused by diode filtering. Residual voltage stage: The circuit does not conduct due to the increase of the thermal expansion resistance of the sample. At this time, the voltage is not zero and the current is.

Figure 4b shows the curve of power, Joule heat and temperature change with time during the Joule thermal shock. At the moment the discharge switch is turned on, the discharge power rapidly rises from 0 to the peak value which can reach up to the level of tens of kilowatts. In the ringback process, the Joule heating power is comparatively low and rises slowly. This is because in the ringback stage, no

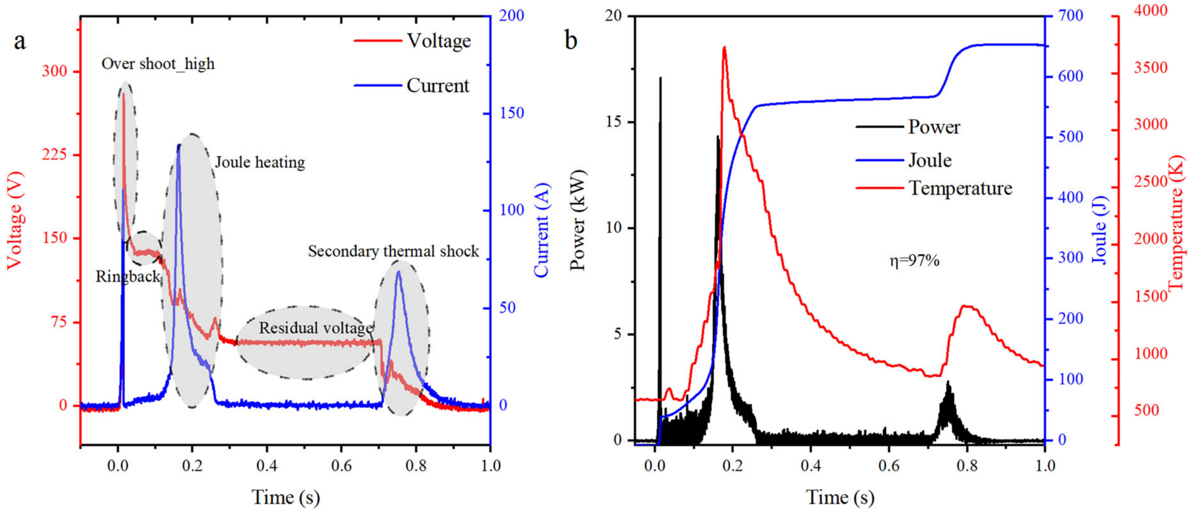

Figure 4. Electrical signal analysis (a) Typical Joule thermal shock process current, voltage and temperature change with time (SCC-150V), (b) Changes in power, Joule heat energy and temperature over time.

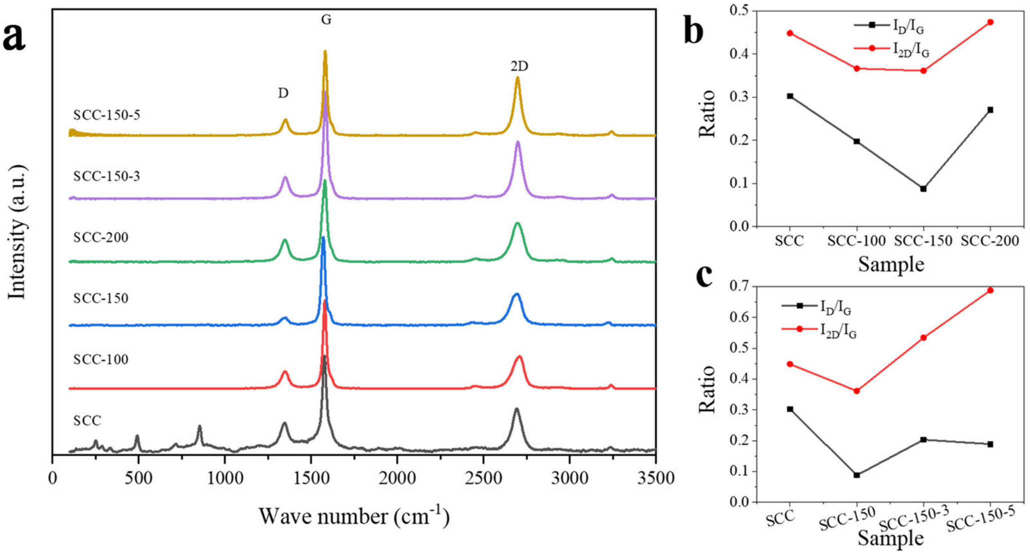

Figure 5. (a) Raman spectra of flash SCC under different flashing voltages and times (b) I_D/I_G and I_{2D}/I_G line graphs of SCC under different flashing voltages (c) I_D/I_G and I_{2D}/I_G line chart of SCC under different flashing times.

discharge channel has ever been formed for the cathode carbon, and accordingly no cathode carbon current. During the thermal shock stage, the voltage begins to drop as the current rises; and due to the conductivity inside the cathode carbon, the electric power rises from 0 again, and then begins to fall after reaching the peak value, which is called the second peak power. The Joule heating power reaches up to 14 kW. When the time reaches 250 ms, the released energy accounts for 81% of the total energy of the capacitor. In addition, due to the strong thermal expansion, the internal resistance of the cathode carbon increases, and the circuit is further disconnected. At this time, there is still some energy stored in the capacitor. Finally, the residual energy undergoes a third Joule thermal shock. It is calculated that during the entire high-temperature thermal shock process, the Joule heat received by the sample accounts for 97% of the energy in the capacitor. The energy conversion rate in the energy storage capacitor during the Joule thermal shock process is much greater than that of the tube furnace. The literature shows that the thermal efficiency in the tube furnace is only about 88–92%, while the energy received by the sample is less than 50%, and the overall efficiency is generally less than 20%.

Table 2. Raman spectra of initial SCC and flashing SCC under different parameters.

Sample	I_D	I_G	I_{2D}	I_D/I_G	I_{2D}/I_G
SCC	921.8	3046	1366	0.3026	0.4486
SCC-100	551.2	2790	1023	0.1975	0.3667
SCC-150	245.4	2785	1007	0.0881	0.3615
SCC-200	701.6	2587	1227	0.2711	0.4741
SCC-150-3	687.7	3385	1809	0.2032	0.5345
SCC-150-5	506.1	2677	1842	0.1891	0.6882

Effect of flashing voltages on purification

The X-ray diffraction was performed on SCC at different flash voltages (100 V, 150 V, and 200 V) to identify the phase structure. As is shown in Figure 3, the broadness of the diffraction centering at 25.4° can be ascribed to the overlap of diffraction from graphite carbon (JCPDS no. 41-1487).[31] Obviously, the high-graphitization characteristics of SCC are not affected by the addition of voltage, which can be further demonstrated in the Raman results later (Fig. 5). Through comparing SCC, SCC-100, SCC-150, and SCC-200, it can be observed that there are many impurities in SCC, such as Al_2O_3, NaF, CaF_2, and aluminosilicate. More specifically, the diffraction peak is significantly weakened after flash joule heating, and its weakening trend slows down as the flashing voltage increases. Hence, the unconditional increase in flash voltage can improve the purification effect to a limited extent. This XRD result shows that the flash joule heating method can effectively remove impurities without affecting the high-graphitization characteristics of SCC. Therefore, to achieve effective purification of SCC, 150 V and 200 V flashing voltage may be the optimal choices.

To find the best process parameters from more aspects, the ordered and disordered graphite crystal structures of SCC under different flash voltages were further evaluated. As is shown in Figure 5a, among the peaks appearing in the Raman spectrum of SCC, 870 cm^{-1} is the Al-OH flexural vibration band,[32] and 725 cm^{-1} is the Al-OH antisymmetric flexural vibration band, 635 cm^{-1} is the Al-OH stretching vibration band, and 528 cm^{-1} is the Al-O-Al vibration band. There are no obvious Raman peaks appearing in the SCC after flashing treatment of below 1000 cm^{-1}, which indicates that the impurities in the SCC have been significantly reduced after flashing treatment. This finding is consistent with the conclusion obtained by XRD. At the same time, the sample shows three typical characteristic peaks of carbon: the D peak (1350 cm^{-1}), G peak (1582 cm^{-1}), and 2 D peak (2700 cm^{-1}).[33] The crystallinity of the sample was reflected by the I_D/I_G values obtained at different flashing voltages by Raman spectroscopy. Table 2 shows the I_D/I_G values of SCC, SCC-100, SCC-150, and SCC-200. Clearly, the values are 0.3026, 0.1975, 0.0881, and 0.2711 respectively, indicating

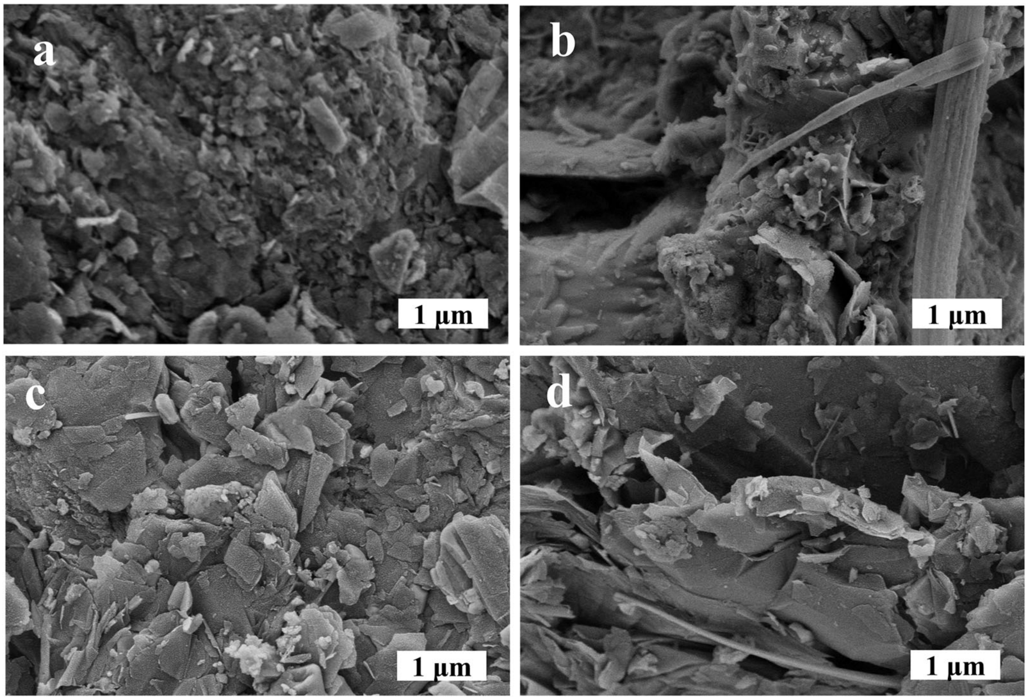

Figure 6. SEM micrograph of SCC before flashing (a); under different flashing voltages, SCC-100(b), SCC-150(c), SCC-200(d).

that the crystallinity of the sample has changed after flash evaporation. As can be seen in Figure 5b, the I_D/I_G values of all the SCC after flashing treatment are lower compared with those of the initial SCC, indicating that the flashing process increased the crystallinity of disordered carbon in SCC. Furthermore, the I_D/I_G values decrease first and then display a rising trend. The disordered structure of SCC increases due to too much input energy when the flash voltage reaches 200 V. All the results indicate that high voltage (200 V) may generate internal defects; the graphitization of the carbon material increases in the SCC as the flashing voltage rises gradually (<150 V). Therefore, considering the preservation of the graphitization structure in the initial SCC, SCC treated with 150 V (SCC-150) was selected for the follow-up experiment.

To better understand the carbon microstructure in the F-SCC, Figure 6 displays the surface morphology of the SCC in the initial state and under different flashing voltages. The number of pores in SCC-100, SCC-150, and SCC-200 has increased. As is shown in Figure 6b, the micropores in the surface of SCC-100 are caused by the impurity which escapes due to the high-temperature sublimation. Then, Figure 5c presents a visibly layered structure of SCC-150, indicating that the graphitized structure is enhanced when the flash voltage is 150 V. Finally, Figure 6d shows the surface topography of SCC-200. As can be seen from the figure, the large grooves may be caused by the impurity which escapes too fast due to the excessive flash voltage. Compared with the initial SCC in Figure 6a, after the high-temperature treatment of flashing (3000 K),[26] the dispersed white substances have disappeared, and the rich layered structure is exposed in Figure 6b–d. These results are consistent with the XRD conclusion that impurity fluorides have been removed and graphitized structure enhanced.

Effect of flashing passes on purification

The effect of flash passes on the efficiency of purification was also investigated. It can be seen from the X-ray diffraction diagram that, as shown above in Figure 3, the impurity elements in SCC gradually decrease as the number of flashing passes increases. When the number of flashing passes increases to 5, the impurity elements in SCC are almost removed completely. Figure 5a and 5c displays the analytical results of the Raman data with different flashing passes. As is shown, although the disordered carbon of SCC increases as the number of passes increases, it is still lower than that of the initial SCC. At the same time, the Raman spectrum can indicate the number of graphite layers by another index: I_{2D}/I_G. The larger the value is, the fewer the graphite layers are. It can be seen from Figure 5c that the layered structure of the initial SCC would be further enhanced while its high-graphitization structure remains unchanged, and that the I_{2D}/I_G value gradually increases as the number of flashing passes increases. This result proves that increasing the number of flashing times is an excellent choice.

The micromorphology of the F-SCC with different passes was further analyzed through SEM. As is shown in Figure 7a and c, the graphite layered structure has been enhanced as the flash joule heating passes increase. At the same time, the micromorphology was also analyzed by EDX, the results of which are displayed in Figure 7b and d. As can be seen, the carbon content of the SCC-150-3 reaches 92.57%, while that of the SCC-150-5 reaches 98.11%, far greater than the carbon content before the flash joule heating. All these results further prove that increasing the number of flash joule heating can improve the effect of purification and enhance the graphite structure.

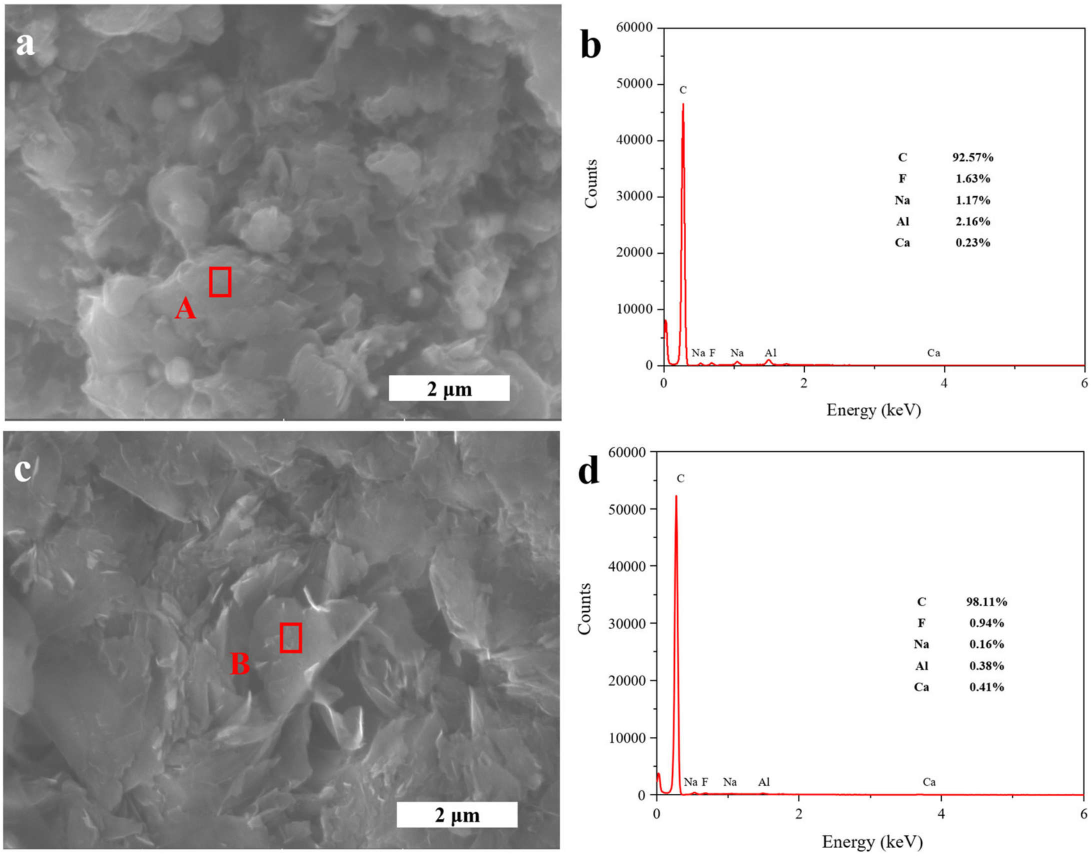

Figure 7. Under different flashing times, SCC-150-3(e) and SCC-150-5(f).

Purification mechanism

In order to study the diffusion mechanism of F, Na and C elements at different temperatures, molecular dynamics simulations were carried out. Figure 8 shows the mean square displacement curve of Na and F in the graphite layer when the temperature is between 300and 5000K. According to the above diffusion coefficient formula, the diffusion coefficients of C, Na, and F can be obtained. It can be seen from the figure that when the temperature is below 3000 K, the diffusion coefficients of C, F and Na are all less than 0.1Å2/ps. When the temperature is over 3000 K, the diffusion coefficients of F and Na begin to increase rapidly. The diffusion coefficients of F and Na are more than 10 times that of C which is always lower than 0.1Å2/ps. It can be seen that under high temperature conditions (3000 K), when NaF diffuses between graphite layers, the diffusion coefficients of Na and F elements are much greater than that of C atoms. This also verifies the reduction of F and Na elements in the XRD and SEM energy spectra observed in the above.

By means of a typical capacitor bank with a capacitance of 60 mF, 120 mg SCC was discharged from 150 to 0 V. The discharge energy can be calculated by the following equation (8):

$$E = \frac{\left(V_1^2 - V_2^2\right) \times C}{2 \times M} \tag{8}$$

where E denotes Energy per gram, V_1 and V_2 stand for Voltage before and after flashing, respectively, C refers to Capacitance, M is Mass per batch.

When the current discharged from the capacitor passes through the SCC, the heat Q (called Joule heat $Q = I^2Rt$) generated in the conductor is proportional to the square of the current (I), the resistance of the conductor (R), and the energization time (t). Due to the non-uniformity of the material properties of the SCC itself, a large amount of heat is generated in a short time by the impurity elements with poor conductivity. Accordingly, the position where the impurity elements and the carbon matrix are in contact would be rapidly heated. The reaction process can be divided into the three stages, namely, Evaporation, Shock, and Collapse. As is shown in Figure 9c, the temperature of the SCC sample subjected to Joule heat rises to 3000 K within 50 ms. Since the temperature of 3000 K greatly exceeds the boiling point of the impurities, the solid impurity elements in the SCC have no time to melt into the liquid state, but directly sublimate into the gaseous state from the solid-state. The high-pressure gas generated at the local position where the impurity contacts the carbon matrix produces strain and stress; when the impurity bubbles diffuse and move, the surrounding solids begin to burst due to their higher pressure, and accumulate inherent characteristics during the inward movement. When the impurity gas finally collapses, the two-way internal inertia of the surrounding solid carbon causes its stress and temperature to increase sharply, and finally the void created by the escape of the impurity element collapses to a small part of its original size. The temperature of the vapor in the bubble may be several thousand Kelvin and the pressure may be several hundred

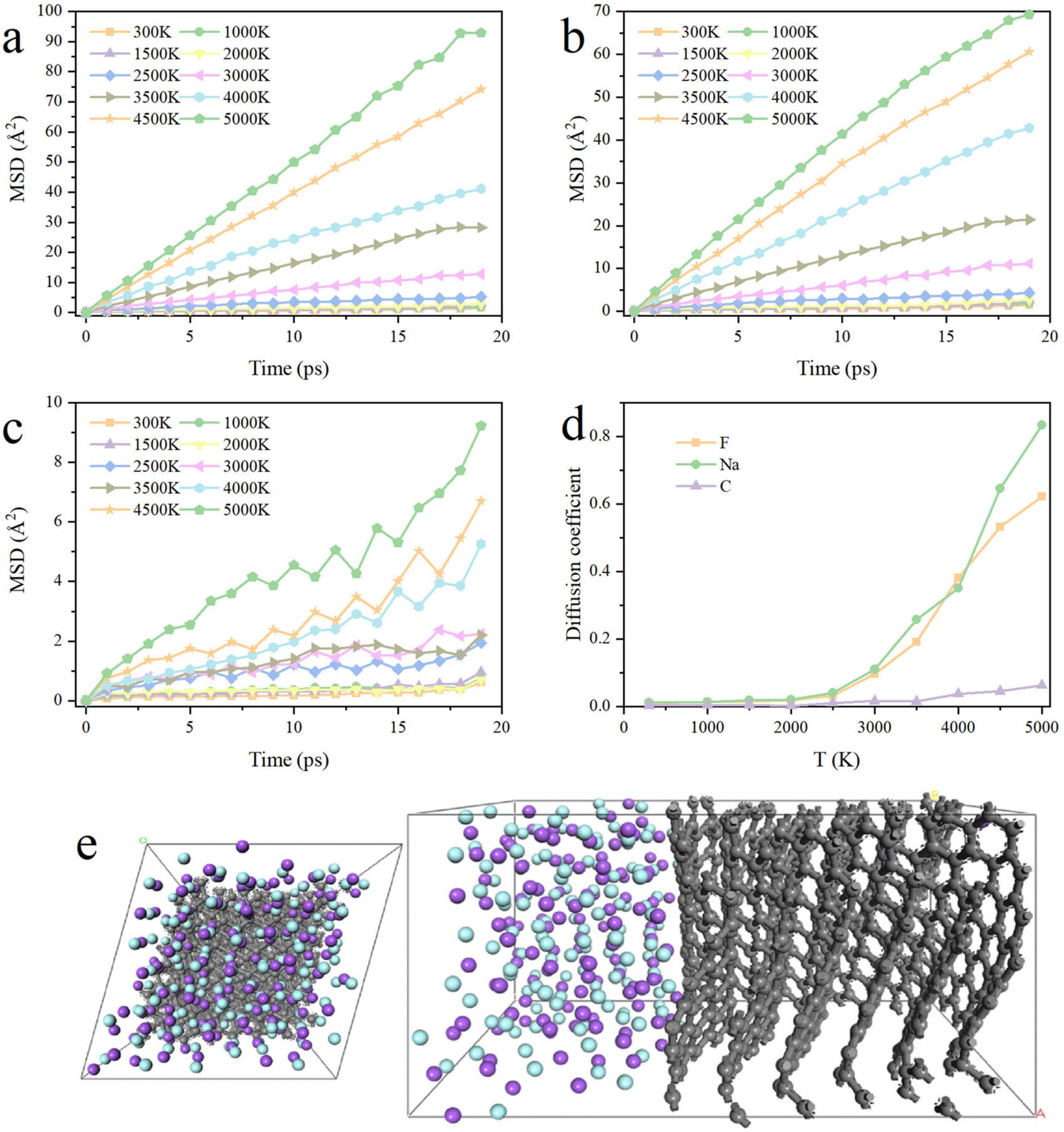

Figure 8. Mean square displacement curves of F(a), Na(b), and C(c) when the temperature is 300 K–5000K, (d) the diffusion coefficient of diffusive elements at different temperatures, (e) molecular dynamics configuration.

atmospheres when the bubble is completely ruptured. In this process, the gas generated by internal impurity elements dissipates into the surrounding solid through a rather violent mechanism, which releases a large amount of energy in the form of sound waves and visible light. Its final pressure is not higher than its vapor pressure, which is called flash joule heating.

Capacitance performance of the F-SCC

F-SCC was used as the electrode material in order to verify the flash joule heating effect. The CV curves of SCC and SCC-150-5 at different scan rates are shown in Figure 10a and b. A pair of obvious redox peaks can be observed, indicating that it has pseudo-capacitance properties. Compared with the case of a high scan rate, the redox peak of the sample is more obvious at a low scan rate. This is because the electrode is more conducive to the adsorption of electrolyte ions at a low scan rate so that the ions in the electrolyte can participate in the reaction more effectively. Compared with the CV curve based on SCC, the CV curve based on SCC-150-5 shows sharper peaks, higher peak intensity, and larger enclosed area, indicating that the electrochemical kinetics of K + intercalation/deintercalation is enhanced. The charge/discharge curves of SCC and SCC-150-5 are shown in Figure 10c and d. On the one hand, the F-SCC improves the electronic conductivity by changing the carbon graphitization structure during the flash joule heating; on the other hand, it also provides adsorption sites to improve the K + intercalation/deintercalation kinetics since a large number of micropores are generated during the escape of impurity elements.

The characteristics of SCC and SCC-150-5 were further analyzed. EIS was performed in the frequency range of 0.01 Hz–100 kHz, with an amplitude of 10 mV. As is shown in Figure 11, the radius of the high-frequency region corresponds to the charge transfer resistance, and the straight line in the low-frequency region represents the diffusion of

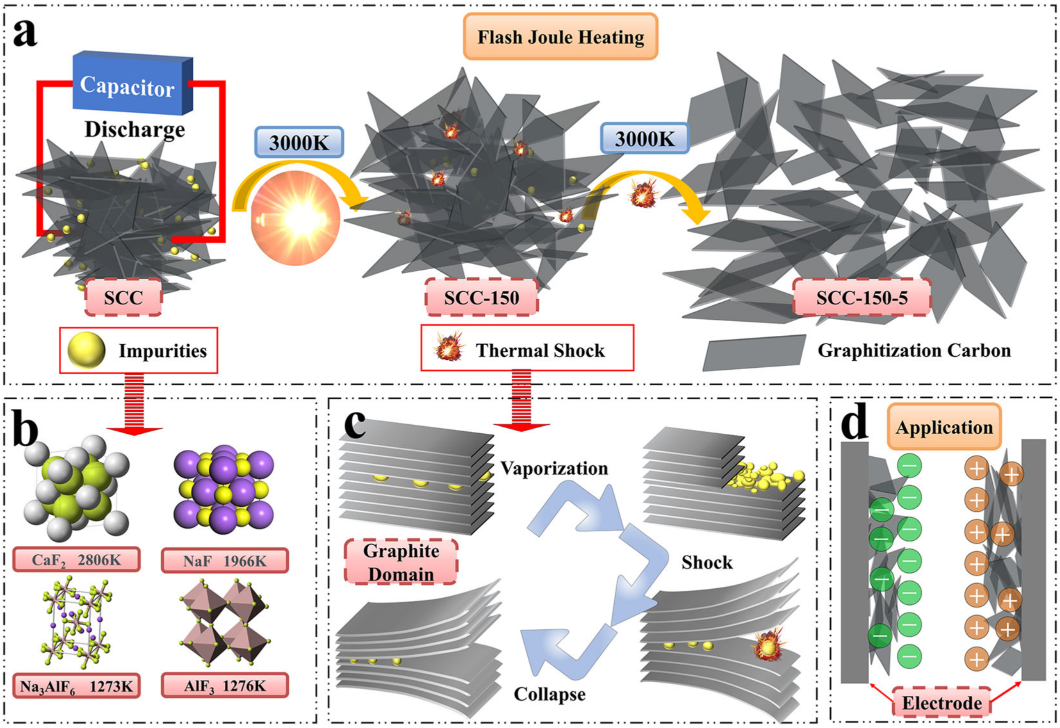

Figure 9. Schematic diagram of the reaction mechanism.

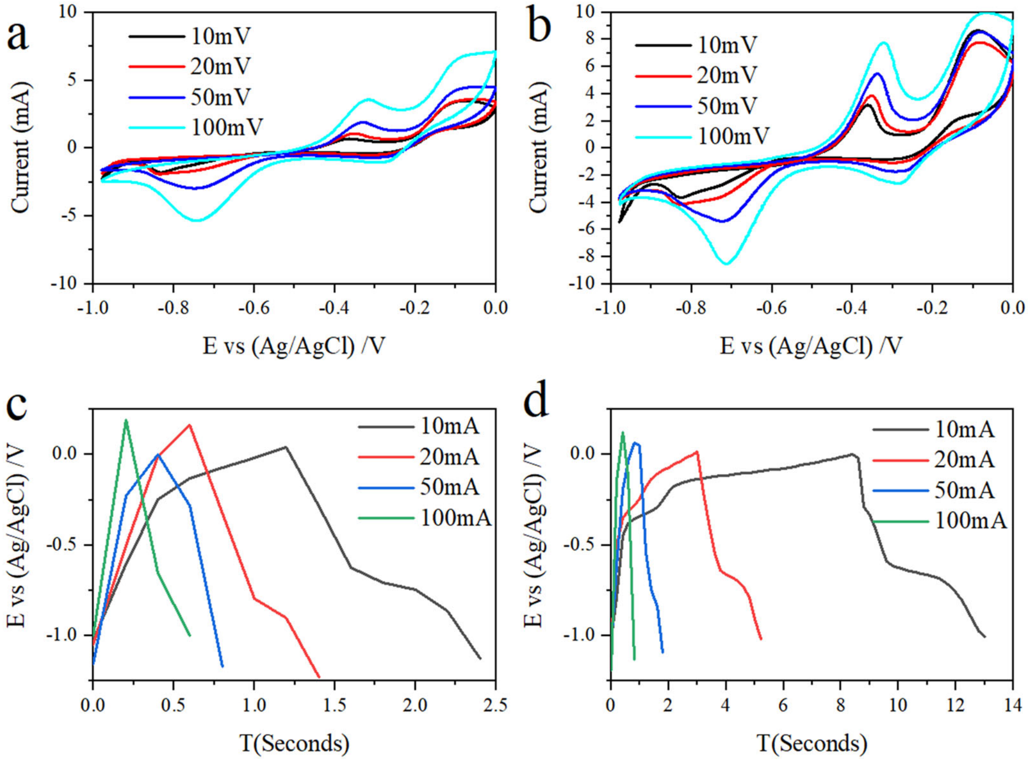

Figure 10. (a–b) CV curves of SCC and SCC-150-5 at different scan rates; (c) Charge and discharge curves of SCC and SCC-150-5 at different scan rates.

K + from the surface into the SCC and SCC-150-5 (Warburg impedance). The smaller radius of the SCC-150-5 indicates that the charge transfer resistance is smaller. The EIS data were fitted by an equivalent circuit, as shown in Figure 11. Rs refers to the uncompensated resistance, including the contact resistance between particles, the electrolyte resistance, and the resistance between the electrode and the current collector. Rct represents the charge transfer resistance, and W represents the Warburg impedance. According to the equivalent circuit, the charge transfer resistance of SCC-150-5 is set to 0.64 Ω, which is much lower than that of SCC (2.36Ω). The small charge transfer resistance of F-SCC can be attributed to the improved conductivity of the conductive network of the sample by flash evaporation.[34]

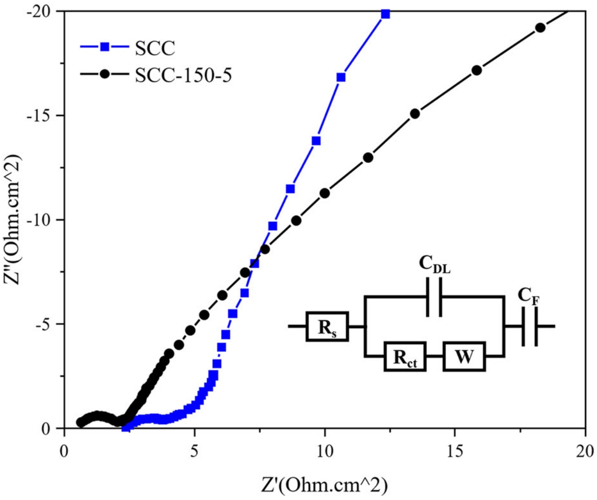

Figure 11. Nyquist plots of SCC and SCC-150-5 in the frequency range of 0.01 Hz–100 kHz.

The micro-expansion graphitization carbon offers an abundant interface and reactive sites, thus enhancing the transfer rate of K + ions.

Conclusion

In conclusion, a facile, rapid, and economical approach based on flash joule heating was proposed to regenerate SCC. The flashing voltage and the removal efficiency of the impurity (F, Na, Al) in the waste cathode carbon were discussed, and the crystal structure and element composition were obtained through characterization of SCC before and after flash joule heating. The results indicate that the removal effect of impurity elements after high-temperature flash joule heating depends on the flash voltage. However, if the voltage is too high, structural defects would arise significantly. Performing multiple flash joule heating at an appropriate voltage of 150 V ($5.62\text{kJ}-^{1}$) can maintain and improve the high graphitization and micro-expansion structure of SCC while effectively increasing the removal of impurity elements. In addition, this paper also studied the application of SCC as an electrode material in supercapacitors before and after flash evaporation. The results show that flash joule heating can improve the capacitance performance of carbon material significantly, because the flash joule heating process (3000 K, 500 ms) improves its graphitization and micro-expansion structure. In this case, the conductivity could be enhanced and abundant interface and reactive sites are available for ions.

Acknowledgments

This work was supported by Fundamental Research Funds for the Central Universities (China University of Mining and Technology) (2019GF08), National Natural Science Foundation of China (51974307), Key Research and Development Project of Xuzhou City (KC21287), the AssistanceProgram for Future Outstanding Talents of China University of Mining and Technology (2021WLJCRCZL038) and the Postgraduate Research & Practice Innovation Program of Jiangsu Province (KYCX21_2426).

Funding

This work was supported by Fundamental Research Funds for the Central Universities (China University of Mining and Technology) (2019GF08), National Natural Science Foundation of China (51974307), Key Research and Development Project of Xuzhou City (KC21287), the Assistance Program for Future Outstanding Talents of China University of Mining and Technology (2021WLJCRCZL038) and the Postgraduate Research & Practice Innovation Program of Jiangsu Province (KYCX21_2426).

ORCID

Pengfei Huang http://orcid.org/0000-0002-5211-6764
Rongtao Zhu http://orcid.org/0000-0003-1248-3567

Data availability statement

The raw/processed data required to reproduce these findings cannot be shared at this time as the data also forms part of an ongoing study.

References

[1] Saevarsdottir, G.; Kvande, H.; Welch, B. J. Aluminum Production in the Times of Climate Change: The Global Challenge to Reduce the Carbon Footprint and Prevent Carbon Leakage. *JOM* **2020**, *72*, 296–308. DOI: 10.1007/s11837-019-03918-6.

[2] Iz, T. P. O. O. S.; Aluminija, P. Sustainable Waste-Treatment Procedure for the Spent Potlining (SPL) from Aluminium Production. *Mater. Technol.* **2019**, *53*, 277–284. DOI: 10.17222/mit.2018.147

[3] Liu, T.; Lin, Z.; Wang, D.; Zhang, M.; Hu, Q.; Tan, L.; Wu, Y.; Zhang, X.; Huang, H.; Wang, J. Aluminum Electrolysis Derivative Spent Cathodic Carbon for Dendrite-Free Li Metal Anode. *Mater. Today Energy* **2020**, *17*, 100465. DOI: 10.1016/j.mtener.2020.100465.

[4] Flores, I. V.; Fraiz, F.; Junior, R. A. L.; Bagatini, M. C. Evaluation of Spent Pot Lining (SPL) as an Alternative Carbonaceous Material in Ironmaking Processes. *J. Mater. Res. Technol.* **2019**, *8*, 33–40. DOI: 10.1016/j.jmrt.2017.11.004.

[5] Yao, Z.; Zhong, Q.; Xiao, J.; Ye, S.; Tang, L.; Wang, Z. Efficient Separation of Fluoride and Graphite Carbon in Spent Cathode Carbon from Aluminum Electrolysis by Mechanical Activation Assisted Alkali Fusion Treatment. *Miner. Eng.* **2021**, *161*, 106717. DOI: 10.1016/j.mineng.2020.106717.

[6] Yuan, J.; Xiao, J.; Li, F.; Wang, B.; Yao, Z.; Yu, B.; Zhang, L. Co-Treatment of Spent Cathode Carbon in Caustic and Acid Leaching Process under Ultrasonic Assisted for Preparation of SiC. *Ultrason. Sonochem.* **2018**, *41*, 608–618. DOI: 10.1016/j.ultsonch.2017.10.027

[7] Sleap, S. B.; Turner, B. D.; Sloan, S. W. Kinetics of Fluoride Removal from Spent Pot Liner Leachate (SPLL) Contaminated Groundwater. *J. Environ. Chem. Eng.* **2015**, *3*, 2580–2587. DOI: 10.1016/j.jece.2015.09.004.

[8] Li, R.; Lu, T.; Xie, M.; Liu, F. Analysis on Thermal Behavior of Fluorides and Cyanides for Heat-Treating Spent Cathode Carbon Blocks from Aluminum Smelters by TG/DSC-MS & ECSA®. *Ecotoxicol. Environ. Saf.* **2020**, *189*, 110015. DOI: 10.1016/j.ecoenv.2019.110015

[9] Yuan, J.; Xiao, J.; Tian, Z.; Yang, K.; Yao, Z. Optimization of Spent Cathode Carbon Purification Process under Ultrasonic Action Using Taguchi Method. *Ind. Eng. Chem. Res.* **2018**, *57*, 7700–7710. DOI: 10.1021/acs.iecr.7b05351.

[10] Xie, M.; Li, R.; Zhao, H.; Liu, W.; Lu, T.; Liu, F. Detoxification of Spent Cathode Carbon Blocks from Aluminum Smelters by Joint Controlling Temperature-Vacuum Process. *J. Clean. Prod.* **2020**, *249*, 119370. DOI: 10.1016/j.jclepro.2019.119370.

[11] Xiao, J.; Yuan, J.; Tian, Z.; Yang, K.; Yao, Z.; Yu, B.; Zhang, L. Comparison of Ultrasound-Assisted and Traditional Caustic Leaching of Spent Cathode Carbon (SCC) from Aluminum Electrolysis. *Ultrason. Sonochem.* **2018**, *40*, 21–29. DOI: 10.1016/j.ultsonch.2017.10.027

[12] Yang, K.; Gong, P.; Tian, Z.; Lai, Y.; Li, J. Recycling Spent Carbon Cathode by a Roasting Method and Its Application in Li-Ion Batteries Anodes. *J. Clean. Prod.* **2020**, *261*, 121090. DOI: 10.1016/j.jclepro.2020.121090.

[13] Yang, K.; Zhao, Z.; Xin, X.; Tian, Z.; Peng, K.; Lai, Y. Graphitic Carbon Materials Extracted from Spent Carbon Cathode of Aluminium Reduction Cell as Anodes for Lithium Ion Batteries: Converting the Hazardous Wastes into Value-Added Materials. *J. Taiwan. Inst. Chem. E* **2019**, *104*, 201–209. DOI: 10.1016/j.jtice.2019.09.012.

[14] Yao, Z.; Zhong, Q.; Xiao, J.; Ye, S.; Tang, L.; Zhang, Z. An Environmental-Friendly Process for Dissociating Toxic Substances and Recovering Valuable Components from Spent Carbon Cathode. *J. Hazard. Mater.* **2021**, *404*, 124120. DOI: 10.1016/j.jhazmat.2020.124120

[15] Yao, Z.; Xiao, J.; Mao, Q.; Wang, G.; Tang, L.; You, Z.; Zhong, Q. Detoxification and Recovery of Spent Carbon Cathodes via NaOH–Na_2CO_3 Binary Molten Salt Roasting–Water Leaching: Toward a Circular Economy for Hazardous Solid Waste from Aluminum Electrolysis. *ACS Sustainable Chem. Eng.* **2020**, *8*, 16912–16923. DOI: 10.1021/acssuschemeng.0c06067.

[16] Li, X.; Yin, W.; Fang, Z.; Liu, Q.; Cui, Y.; Zhao, J.; Jia, H. Recovery of Carbon and Valuable Components from Spent Pot Lining by Leaching with Acidic Aluminum Anodizing Wastewaters. *Metall. Mater. Trans. B* **2019**, *50*, 914–923. DOI: 10.1007/s11663-018-1485-3.

[17] Yaowu, W.; Jianping, P.; Yuezhong, D. Separation and Recycling of Spent Carbon Cathode Blocks in the Aluminum Industry by the Vacuum Distillation Process. *JOM* **2018**, *70*, 1877–1882. DOI: 10.1007/s11837-018-2858-4.

[18] Xie, M-z.; Zhao, H-l.; Wu, Z-g.; Liu, W.; Li, R-b.; Liu, F-q. Study on Kinetics of Vacuum Heat Treatment Process of the Spent Cathode Carbon Blocks from Aluminum Smelters. *J. Sustain. Metall.* **2020**, *6*, 715–723. DOI: 10.1007/s40831-020-00311-5.

[19] Agrawal, A.; Kumar, C.; Meshram, A. Recovery of Carbon Rich Material:–Recycling of Spent Pot Lining: A Review. *Mater. Today: Proc.* **2021**, *46*, 1526–1531. DOI: 10.1016/j.matpr.2021.01.143.

[20] Mahmoudi, M. M.; Nasseri, S.; Mahvi, A. H.; Dargahi, A.; Khubestani, M. S.; Salari, M. Fluoride Removal from Aqueous Solution by Acid-Treated Clinoptilolite: Isotherm and Kinetic Study. *Desalination Water Treat.* **2019**, *146*, 333–340. DOI: 10.5004/dwt.2019.23625.

[21] Kondratiev, V.; Rzhechitskiy, E.; Ershov, V.; Bogdanov, Y.; Karlina, A. Results of Carrying out of Researches with Revealing of Technological Parameters of Processes of Recycling and Neutralization of the First and Second Cut of the Spent Lining of Electrolyzers for Reception of Aluminum Fluoride. *Int. J. Appl. Eng. Res.* **2017**, *12*, 12801–12808.

[22] Wang, G.; Oswald, S.; Löffler, M.; Müllen, K.; Feng, X. Beyond Activated Carbon: Graphite-Cathode-Derived Li-Ion Pseudocapacitors with High Energy and High Power Densities. *Adv. Mater.* **2019**, *31*, 1807712. DOI: 10.1002/adma.201807712.

[23] Brezesinski, T.; Wang, J.; Tolbert, S. H.; Dunn, B. Ordered Mesoporous Alpha-MoO_3 with Iso-Oriented Nanocrystalline Walls for Thin-Film Pseudocapacitors. *Nat. Mater.* **2010**, *9*, 146–151. DOI: 10.1038/nmat2612

[24] Stanford, M. G.; Bets, K. V.; Luong, D. X.; Advincula, P. A.; Chen, W.; Li, J. T.; Wang, Z.; McHugh, E. A.; Algozeeb, W. A.; Yakobson, B. I.; Tour, J. M. Flash Graphene Morphologies. *ACS Nano* **2020**, *14*, 13691–13699. DOI: 10.1021/acsnano.0c05900

[25] Algozeeb, W. A.; Savas, P. E.; Luong, D. X.; Chen, W.; Kittrell, C.; Bhat, M.; Shahsavari, R.; Tour, J. M. Flash Graphene from Plastic Waste. *ACS Nano* **2020**, *14*, 15595–15604. DOI: 10.1021/acsnano.0c06328

[26] Luong, D. X.; Bets, K. V.; Algozeeb, W. A.; Stanford, M. G.; Kittrell, C.; Chen, W.; Salvatierra, R. V.; Ren, M.; McHugh, E. A.; Advincula, P. A.; et al. Gram-Scale Bottom-up Flash Graphene Synthesis. *Nature* **2020**, *577*, 647–651. DOI: 10.1038/s41586-020-1938-0

[27] Molaiyan, P.; Witter, R. Surface Defect-Enhanced Conductivity of Calcium Fluoride for Electrochemical Applications. *Mater. Design. Process. Commun.* **2019**, *1*, e44. DOI: 10.1002/mdp2.44.

[28] Taherialekouhi, R.; Rasouli, S.; Khosravi, A. An Experimental Study on Stability and Thermal Conductivity of Water-Graphene Oxide/Aluminum Oxide Nanoparticles as a Cooling Hybrid Nanofluid. *Int. J. Heat. Mass. Transf.* **2019**, *145*, 118751. DOI: 10.1016/j.ijheatmasstransfer.2019.118751.

[29] Nie, Y.; Guo, X.; Guo, Z.; Tang, J.; Xiao, X.; Xin, L. Defluorination of Spent Pot Lining from Aluminum Electrolysis Using Acidic Iron-Containing Solution. *Hydrometallurgy* **2020**, *194*, 105319. DOI: 10.1016/j.hydromet.2020.105319.

[30] Liu, J.; Zhang, L.; Xu, L. Elastic, Electronic Structure, and Optical Properties of Orthorhombic Na 3 AlF 6: A First-Principles Study. *Ionics* **2018**, *24*, 1377–1383. DOI: 10.1007/s11581-017-2285-5.

[31] Sari, S. N.; Melati, A. Facile Preparation of Carbon Nanofiber from Banana Peel Waste. *Mater. Today Proc.* **2019**, *13*, 165–168. DOI: 10.1016/j.matpr.2019.03.208.

[32] Pazourková, L.; Peikertová, P.; Hundáková, M.; Martynková, G. S. Preparation of Calcium Deficient Hydroxyapatite on the Montmorillonite Substrate: Structure and Morphology. *Mater. Today Proc.* **2020**, *37*, 35–41. DOI: 10.1016/j.matpr.2020.02.927

[33] Huang, P.; Zhu, R.; Li, C.; Wang, X.; Wang, X.; Zhang, X. Effect of Graphene Concentration on Tribological Properties of Graphene Aerogel/TiO_2 Composite through Controllable Cellular-Structure. *Mater. Design* **2020**, *188*, 108468. DOI: 10.1016/j.matdes.2020.108468.

[34] Bi, Z.; Kong, Q.; Cao, Y.; Sun, G.; Su, F.; Wei, X.; Li, X.; Ahmad, A.; Xie, L.; Chen, C.-M. Biomass-Derived Porous Carbon Materials with Different Dimensions for Supercapacitor Electrodes: A Review. *J. Mater. Chem. A* **2019**, *7*, 16028–16045. DOI: 10.1039/C9TA04436A.

Appendix A

The sample stage is shown in Figure A1, the quartz tube (1) contains the sample (2) waste cathode carbon powder; the two ends of the quartz tube (1) are sealed with graphite blocks (3), and the electrode rods are installed symmetrically (10); The electrode rods (10) are copper electrodes, which are respectively installed in sliding fit with the rubber plate (7) of the sample stage; the electrode rods (10) are located on both sides of the rubber plate (7) through the limit nuts (9). A gasket (5) is fixedly installed, and a spring (6) structure is arranged

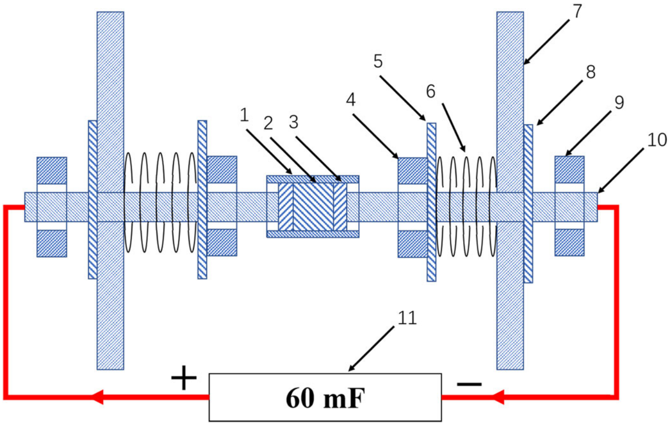

Figure A1. Schematic diagram of sample stage (1. Quartz tube 2. Sample 3. Graphite block 4. Fixing nut 5. Gasket 6. Spring 7. Rubber sheet 8. Gasket 9. Limit nut 10. Electrode 11. capacitance).

between the gasket on the side of the quartz tube 1 and the rubber plate (7); the electrode rod (10) is connected to the capacitor (11) Connection; when the high temperature and high thermal shock system thermally impacts the waste cathode carbon powder in the quartz tube (1), the generated high-temperature gas impacts the graphite block (3), and the electrode rod (10) slides to both sides along the rubber plate (7), Allowing the gas to escape during the high temperature thermal shock, and changing the pre-tightening force by compressing the spring (6) to increase the conductivity of the sample (2).

The circuit diagram of the device is shown in Figure A2, C1–C10 is a capacitor combination consisting of 10 aluminum electrolytic capacitors with a capacitance of 6 mF 450 V; R1–R10 are 10 200 kΩ resistors; R1–R10 are 10 resistors with a resistance value of 200kΩ; R13 is a 5 kΩ Resistance; R14 is 100 kΩ resistance; S1–S10 is 400 V, 6 A discharge and charge switch circuit breaker; S11 is 5 V, 1 A relay switch; S12–S13 is 277 V, 10 A capacitor switch circuit breaker; DC425V is 425 V DC power supply; DC24V. It is a 24 V DC power supply; D1–D2: 1200 V, 560 A diode; L1 is a 24 mH inductor; Ry is a 900 V, 500 A mechanical relay; PLC is Siemens S7200-CPU 226.

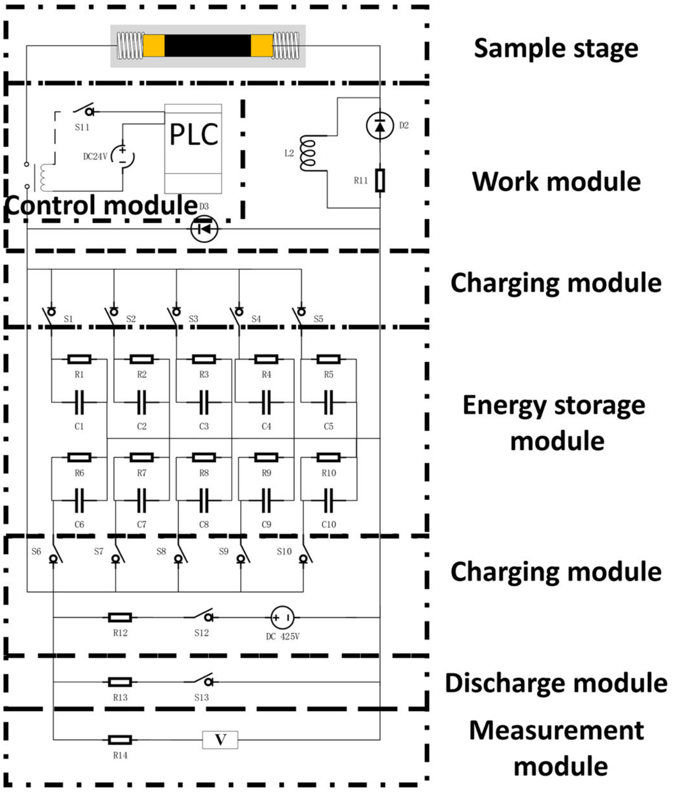

Figure A2. Device circuit diagram.

The Joule heating device includes a control module, a charging module, a discharging module, a working module, an energy storage module, and a measurement module. The control module includes a controller PLC and an actuator relay; the charging module includes a charging power supply, a capacitor, a charging resistor, and a charging switch. The charging resistor is to prevent the charging current from being too large and is connected in series in the charging circuit; the discharging module includes a discharging resistor, a discharging switch, and a capacitor, and when it stops working, the energy in the capacitor is discharged through the resistor to ensure safety; The energy storage module is mainly composed of a capacitor; the working module includes a sample stage, a reaction kettle, an inductor, a diode, and a resistance; the measurement module includes a voltage, resistance, and temperature and pressure measuring meter.

The PLC controls the opening and closing of the switch S12, and uses 425 V dynamic current to charge the capacitor C1–C10 of the charging module; after the C1-C10 capacitor combination is charged to the specified voltage, the switch S12 and the PLC control switch S11 pass, The cathode carbon powder (2) is subjected to Joule thermal shock from both ends of the quartz tube (1) through the electrode rod (10) connected to the circuit; During the thermal process, the gas is allowed to escape during the high-temperature shock thermal shock, and the compression elastic device (6) is used to pre-tighten the sample to increase the conductivity of the sample; PLC performs 1–5 Joule thermal shocks according to the set number of impacts; After the Joule thermal shock is completed, PLC controls the thermal radiation of the discharge module and prepares to enter the Joule thermal shock program. In the above process, S1–S13 and Ry are correspondingly opened or closed to realize charging and discharging operations. The inductance L2 reduces the peak current in the circuit and reduces the requirements of the circuit. Combined with the function of the diode D2, it can effectively eliminate the oscillation characteristics of the circuit. The diodes D2 and R11 can release the residual electricity in L2 after the thermal expansion resistance of the sample increases.

The self-made signal test system includes three parts: signal acquisition, AD conversion and digital signal processing. Signal acquisition: including temperature sensor (Shanghai Electric, IRTD-3200) Hall current sensor (Senshe, CHB500SG) Hall voltage sensor (Senshe, CHV-25P). Voltage, current and temperature signals ware converted into electrical signals through corresponding sensors; AD conversion: the electrical signal was converted into a digital signal through the Pcie-6321 data acquisition card; Digital signal processing: recorded and displayed by the labview program.

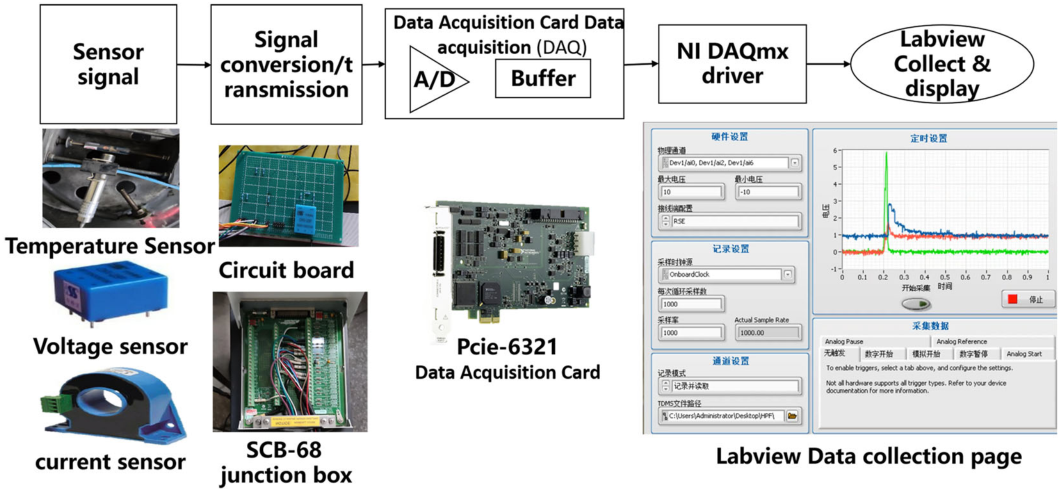

物理通道: Dev1/ai0, Dev1/ai2, Dev1/ai6

最大电压: 10

最小电压: -10

接线端配置: RSE

采样时钟源: OnboardClock

每次循环采样数: 1000

采样率: 1000

Actual Sample Rate: 1000.00

记录模式: 记录并读取

TDMS文件路径: C:\Users\Administrator\Desktop\HPF\

To enable triggers, select a tab above, and configure the settings.

Not all hardware supports all trigger types. Refer to your device documentation for more information.

Figure A3. Signal test system.